ELSEVIER

Journal of Applied Geophysics 43 (2000) 15–32

JOURNAL OF APPLIED GEOPHYSICS

www.elsevier.nl/locate/jappgeo

Fast Imaging of TDEM data based on S-inversion

Efthimios Tartaras [a,*], Michael S. Zhdanov [a,1], Kazushige Wada [b], Akira Saito [b], Toshiaki Hara [c]

[a] *Department of Geology and Geophysics, College of Mines and Earth Sciences, University of Utah, 135 S 1460 E., Room 719, Salt Lake City, UT 84112 USA*

[b] *Mindeco, Japan*

[c] *Toda, Japan*

Received 11 December 1998; accepted 16 July 1999

Abstract

Fast S-inversion is a method of interpretation of time-domain electromagnetic (TDEM) sounding data using the thin sheet model approach. Within the framework of this method, the electromagnetic (EM) response measured at the surface of the earth at every time delay is matched with that of a thin sheet model. The conductivity change with depth is obtained using the conductance, S, and depth, d, of the equivalent thin sheet. We analyze two different numerical techniques, the *differential S-transformation* and the *regularized S-inversion*, to determine the parameters of the thin sheet. The first technique is a direct differential transformation of the observed data into conductance and depth values. It is fast and requires no iterations or starting model. The second technique uses a regularized inversion scheme to fit the measured response with that of a thin sheet. In both techniques, the retrieved conductance values are differentiated with respect to depth to obtain the conductivity change with depth. We apply S-inversion to three-dimensional synthetic data and we successfully locate the local conductors. We also demonstrate a case history by interpreting TDEM data obtained at the Nojima fault zone in Japan. The results clearly indicate the location of the fault zone.

Keywords: Electromagnetic methods; Transient methods; Conductivity; Inverse problem

1. Introduction

Over the last two decades, there has been a dramatic surge of interest in transient methods of exploration. The time-domain electromagnetic (TDEM) sounding method is now one of the major tools for electromagnetic (EM) exploration. However, interpretation of TDEM data is still a challenging task. The reason is that responses of three-dimensional (3-D) models of the earth are complicated and expensive to calculate and, therefore, full 3-D inversion is not feasible yet.

TDEM data are most often interpreted using conventional one-dimensional (1-D) inversion techniques, or approximate, fast imaging techniques. 1-D inversion is based on fitting the theoretical response from a 1-D structure to the real data in a least-square sense. It is subsequently applied to every survey point. Combin-

* Corresponding author. Fax: +1-801-581-7065; E-mail: tartaras@mines.utah.edu

[1] E-mail: mzhdanov@mines.utah.edu.

0926-9851/00/$ - see front matter
PII: S0926-9851(99)00030-0

ing 1-D images together forms the conductivity–depth image. 1-D inversion techniques are mathematically rigorous, but still quite time-consuming and biased by 3-D effects. Several fast resistivity imaging techniques have been developed in recent years (Lee, 1977; Barnett, 1984; Macnae and Lamontagne, 1987; Nekut, 1987; Eaton and Hohmann, 1989; Fullagar, 1989; Smith et al., 1994; Wolfgram and Karlik, 1995). The majority of these methods are based on equating the transient response, measured at the surface of the earth, to the EM field in free space of current filament images of the source. This approach was based on the pioneering work of Nabighian (1979), which describes the transient currents diffusing into the earth as similar to a system of "smoke rings" blown by the transmitting loop into the earth. This idea was further developed by Raiche and Gallagher (1985) who described the vertical diffusion velocity of the EM field through a homogeneous half-space earth model. The calculation of the conductivity, σ, in most of the existing fast imaging methods is based on expressions derived from this diffusion velocity. Therefore, the resulting conductivity distribution tends to be rather smooth. We would often like, however, to calculate the conductivity based on a model that can more accurately approximate local conductors in the earth.

Sidorov and Tikshaev (1969) suggested a different approach for fast imaging of TDEM data. The basic idea is that instead of considering an equivalent homogeneous half-space, like in the traditional apparent resistivity definition, one can introduce equivalent conductive thin sheet within the free space. We can determine the apparent conductance $S_a(t)$ as the conductance of the thin sheet located at the depth, d, within the free space, which generates theoretical EM response equal to the observed TDEM response at some time delay, t. This apparent conductance can be treated as the total conductance of the sequences of the layers within the depth range of EM field penetration inside the earth for a given time delay.

A similar approach was later introduced independently by Liu and Asten (1993) for conductance–depth imaging of transient EM data. It is based on the calculation for every time channel of the conductance, S, and depth, d, of the equivalent thin sheet, which can be used to determine vertical conductivity profiles of the geoelectrical cross-section. Asten (1998) discusses the merits of a conductance–depth imaging scheme for the identification of weak conductors under conductive overburden.

In this paper, we present further development and analysis of the method. We study two techniques, the differential S-transformation and the regularized S-inversion, for the calculation of the thin sheet parameters. We apply S-inversion to 3-D synthetic data. We also demonstrate a case history by interpreting TDEM data obtained at the Nojima fault zone in Japan. The results clearly show the location of the Nojima fault zone and delineate another interesting faulting zone in the middle of the profiles.

Thus, the main goal of this paper is to show that S-inversion is an efficient and stable method for fast imaging of TDEM data.

2. Principles of S-inversion

S-inversion is a fast-imaging technique for TDEM data interpretation based on the thin sheet model approach (Tartaras and Zhdanov, 1996). The foundations of the thin sheet model approach for conductivity–depth imaging lie in the theory of EM induction in thin conducting layers. This theory was first developed by Price (1949) and Sheinmann (1947). Their model has become known as the *thin sheet* model. The theory for such models was extended by Tikhonov, Dmitriev, Berdichevsky, and Zhdanov to cases in which layers with nonzero thickness, d, could be included (Berdichevsky and Zhdanov, 1984; Singer and Green, 1998).

Let us examine the behavior of a step-induced transient magnetic field excited by a ver-

tical magnetic dipole for a medium which consists of a single conducting sheet in an otherwise insulating full space. The thin sheet lies at depth, d, and has uniform integral conductance S (Fig. 1). We can assume that an EM field is caused by current flowing in a loop of wire lying in the horizontal plane forming a vertical-axis magnetic dipole with a moment M at the surface of the earth. The waveform of the current flowing in the coil, I, is that of a Heaviside function (instantaneous change in level), $I = I_o H(t)$. We wish to find the field from this source at the surface of the earth. It is proven (Sidorov and Tikshaev, 1969; Zhdanov and Keller, 1994) that the time-rate of change of the magnetic induction vector (the physical quantity measured with an induction coil receiver) is:

$$\left.\frac{\partial B_z(t)}{\partial t}\right|_{z=0} = -\mu_o \frac{M\delta(t)}{4\pi r^3} + \frac{M(d+\tau)}{\pi S} \times \frac{\left[-9r^2 + 24(d+\tau)^2\right]}{\left[r^2 + 4(d+\tau)^2\right]^{7/2}}, \quad (1)$$

where r is the distance between observation point and the source, μ_0 is the magnetic permeability of the free space, and $\tau = t/\mu_o S$.

Note that the conductance S of one horizontal layer is the inverse resistance to the currents flowing horizontally through the layer. Integral conductance of the sequence of the N layers is simply the sum of the individual conductances:

$$S = \sum_{i=1}^{N} \frac{h_i}{\rho_i},$$

where h_i, ρ_i are thicknesses and resistivities of the layers.

In the case of continuous variations of the conductivity with depth, we can define the conductance S by the formula:

$$S = \int_0^{\zeta} \frac{dz}{\rho(z)} = \int_0^{\zeta} \sigma(z)dz, \quad (2)$$

where ζ is the effective depth of EM field penetration, and $\rho(z)$ and $\sigma(z)$ are variable with the depth resistivity and conductivity (Zhdanov and Keller, 1994). It is assumed in the integral that we estimate the integral conductance of the layers within the depth interval from 0 to ζ.

We can see from the above Eq. (1) that the spreading of the internal part of the magnetic field into the medium at the very first instant of time is markedly nonuniform. The field at a given point on the surface depends not only on the model parameters (i.e., the conductance, S, and the depth, d, of the thin sheet) but also on the distance, r, of that point from the source. But as time progresses, the internal field becomes more uniform in its spreading into the medium. In this respect, at sufficiently late times and sufficiently near the source, such that $r^2 \ll (d+\tau)^2$, Eq. (1) simplifies to:

$$\left.\frac{\partial B_z(t)}{\partial t}\right|_{z=0} \approx \frac{-3M}{16\pi S(d+\tau)^4}. \quad (3)$$

Now the field depends only on the thin sheet parameters and not on the distance, r.

Note that the late time approximation can be used for central-loop soundings survey, because the required condition $r^2 \ll (d+\tau)^2$ always holds if $r = 0$. In general case of arbitrary transmitter–receiver separations, the full formula (1) can be used.

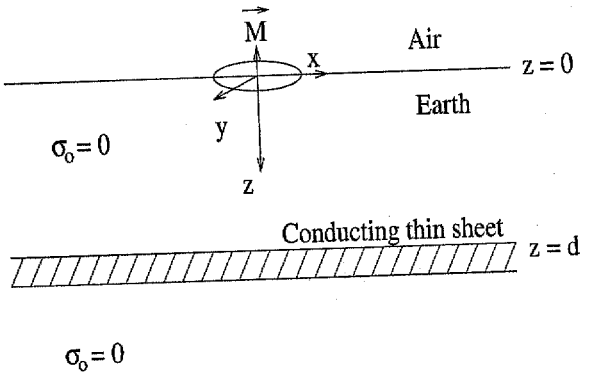

Fig. 1. Thin sheet model.

The basic idea of the S-inversion method can be described as follows. Traditional approach to the interpretation of electrical sounding methods uses the concept of apparent resistivity. This concept is based on the simple model of a homogeneous half-space. We introduce the apparent resistivity, ρ_a, as the resistivity of the homogeneous half-space which generates theoretical EM response equal to the observed EM response for some frequency ω or for some time delay, t (for a TDEM field). Thus, the apparent resistivity is a function of frequency $[\rho_a(\omega)]$ or time $[\rho_a(t)]$. The plots $\rho_a(\omega)$ or $\rho_a(t)$ are called apparent resistivity curves. In EM sounding theory, there are several well-known techniques which transform the apparent resistivity curves into resistivity–depth images. The idea is simple. We can introduce the effective depth of penetration, ζ, of EM field in the earth, which depends on frequency or time and is actually related to the skin-depth. After some algebraic transformation one can derive the function of the apparent resistivity vs. the effective depth $\rho_a(\zeta)$. This curve describes the 1-D image beneath the sounding point. By combining these 1-D curves together for different observation points we construct the resistivity–depth image $\rho_a(x,\zeta)$, where x is the position of the observation point along the profile, and ζ is the effective depth of EM field penetration, which varies from close to zero to some depth, D, thus outlining the geoelectrical cross-section. Parasection $\rho_a(x,\zeta)$ is usually treated as the fast image of the real geoelectrical cross-section. It is not an inversion result, but a simple transformation of the observed sounding curves into depth sections. Unfortunately, this transformation provides smooth images that might not always be representative of the real geological cross-sections, especially in the presence of strong local conductors.

In the case of S-inversion instead of considering equivalent homogeneous half-space, we introduce equivalent conductive thin sheet within the free space. We can determine the apparent conductance $S_a(t_1)$ as the conductance of the thin sheet located at the depth d_1 within the free space, which generates theoretical EM response equal to the observed TDEM response for some time delay t_1. This apparent conductance can be treated as the total conductance of the sequences of the layers within the depth range of EM field penetration inside the earth for the given time delay. It is well known that the depth of TDEM field penetration is proportional to the square root of time t. With increasing time delay, the depth of penetration increases, therefore the apparent total conductance increases as well, because it is a monotonic function of the depth. Therefore, for the next time delay t_2, we will find another equivalent thin sheet with the larger conductance $S_a(t_2) > S_a(t_1)$ and the larger depth $d_2 > d_1$. Thus, the apparent conductance is a function of time $S_a(t)$. The plot $S_a(t)$ is called the apparent conductance curve. For every time delay, we find not only the conductance but also the depth, d, of the equivalent thin sheet. Therefore, we can easily generate the function of the apparent conductance vs. the effective depth $S_a(d)$. This curve theoretically should be a monotonically increasing curve, because the conductance increases with the depth. At the same time, the integral conductance of the geoelectrical cross-section is connected with the vertical conductivity distribution $\sigma(z)$ by the simple formula (Eq. 2) shown above. Therefore, by differentiating the conductance–depth curve we can finally obtain the conductivity change with the depth:

$$\sigma(d) = S'(d). \tag{4}$$

This curve describes the 1-D image beneath the sounding point. By combining these 1-D curves together for different observation points, we obtain the conductivity–depth image $\sigma(x,d)$, where x is the position of the observation point along the profile, and d is the effective depth of the equivalent thin sheet, which varies from some minimum depth (dependent on the earliest time delay recorded, and on near-surface conductivity) to some depth, D, thus outlining the geoelectrical cross-section. In this way, based

on the observed time derivatives of the vertical component of the magnetic induction vector, we can obtain the conductance–depth curve.

2.1. Differential S-transformation

Sidorov and Tikshaev (1969) suggested a simple approach to the solution of the inverse problem, which is called the "differential S-transformation". The method directly transforms the observed time derivatives of the vertical component of the magnetic induction vector into conductance–depth values.

If we consider the output of an ideal receiver loop $V = -\Sigma n(\partial B_z/\partial t)$, where Σ and n are the area and the number of turns of the receiver coil, respectively, then from Eq. (3), we have:

$$|V| = \frac{3M\Sigma n}{16\pi S}\frac{1}{(d+\tau)^4}. \quad (5)$$

Differentiating the above equation with respect to time, we obtain:

$$|V|' = -\frac{3M\Sigma n}{4\pi S^2\mu_o}\frac{1}{(d+\tau)^5}. \quad (6)$$

By raising Eq. (5) to the 5/3 power and Eq. (6) to the 4/3 power and finally dividing the two resulting equations, we arrive at the following formula for calculation of the conductance:

$$S = \frac{16\pi^{1/3}}{(3M\Sigma n)^{1/3}\mu_o^{4/3}}\frac{(|V|)^{5/3}}{(|V|')^{4/3}}. \quad (7)$$

On the other hand, by dividing Eqs. (5) and (6) and solving for d, we can calculate the depth from the following formula:

$$d = \frac{1}{\mu_o S}\left(-\frac{4|V|}{|V|'} - t\right), \quad (8)$$

where $|V|'$ is the time derivative of the measured voltage $|V|$. We obtain the time derivatives of the observed voltages using a numerical differentiation scheme that computes a first order derivative for the provided TDEM data using polynomial interpolation.

From Eqs. (7) and (8), we can obtain efficiently the conductance–depth curve based on the observed time derivatives of the vertical component of the magnetic induction vector. Then, we numerically differentiate the conductance curve with respect to depth using the same differentiation scheme to obtain conductivity as a function of depth.

Because numerical differentiation enhances noise, data should be smoothed prior to and following differentiation. We apply a moving-average low-pass filter to our data. In particular, we use a five-point Hanning filter which we convolve with our data set in the logarithmic space.

The differential S-transformation is very fast and has the advantage that it employs no iterative computations and, especially, no starting model. On the other hand, it has the drawback that it requires a differentiation scheme, which can generate additional noise in the interpretation results, to transform the observed data to depth and conductance values. Another limitation of this technique is related to the use of the late time approximation (3) for magnetic field.

2.2. Regularized S-inversion

Another approach to the solution of the inverse problem is based on full inversion with respect to the thin sheet parameters S and d. The principles of this approach have been discussed by Liu and Asten (1993). We use an adaptive regularized Newton inversion scheme to determine the thin sheet parameters.

Using Eq. (5) for the calculation of the late-time field response, we fit the data measured at adjacent time channels in order to obtain the depth and conductance of a thin sheet. Since we invert for two parameters, S and d, we can use data from just two adjacent time channels for each inversion. However, to make the solution more stable to the noise, we select several adjacent time channels (usually 4 or 5) that form a sliding time window $(t - \Delta t/2, t + \Delta t/2)$,

where Δt is the width of the window (Fig. 2). Hence, the obtained values for the conductance and depth of the thin sheet are actually the averaged values of the two parameters over the selected time window. Every fixed position of the sliding window center t corresponds to the specific depth, ζ, of the EM field penetration in the earth. We solve numerically the inverse problem and find the parameters of the thin sheet, $S(\zeta)$ and $d(\zeta)$, which is equivalent to the conducting thickness of the earth above the depth of penetration ζ. When we move the sliding time window to later times, the new inverted parameters of the thin sheet correspond to the total conductance of the earth layer above the new depth of penetration ζ'. Obviously, we should obtain monotonically increasing curves $S(\zeta)$ and $d(\zeta)$, which correspond to the model of a "sinking" thin sheet with increasing total conductance. These values, $S(\zeta)$ and $d(\zeta)$, when plotted together, form the conductance–depth curve.

We use the adaptive regularized Newton method for the solution of the inverse problem (Zhdanov and Keller, 1994). The most notable difference between our method and the one applied by Liu and Asten (1993) is the use of regularization, which is important in order to stabilize the inversion, especially when we are dealing with noisy data.

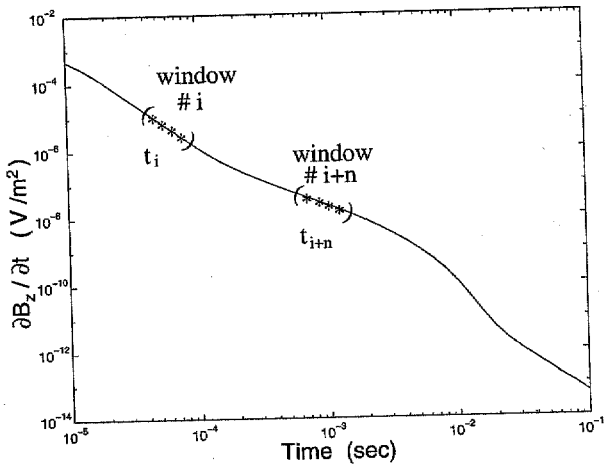

Fig. 2. Inversion of successive data windows.

In the adaptive regularized Newton method, we minimize the parametric functional, P^{α}:

$$P^{\alpha}(m) = \phi(m) + \alpha Q(m), \tag{9}$$

which is a function of the model, m, and also depends on the value of the regularization parameter α. $\phi(m)$ is the misfit functional:

$$\phi(m) = \|R(m)\|^2, \tag{10}$$

and $Q(m)$ is the stabilizing functional:

$$Q(m) = \|m - m_{\text{apr}}\|^2, \tag{11}$$

which is used in order to ensure the stability of the inversion algorithm. In the above equations, $R(m)$ denotes the residual:

$$R(m) = A(m) - A_{\text{o}}, \tag{12}$$

A is the forward operator, A_{o} is the data we are trying to fit, m_{apr} is the a priori model, and $\|\ldots\|$ denotes the least squares norm.

In the framework of the Newton method, the model m_{n+1} in the $(n+1)$th iteration is given by:

$$m_{n+1} = m_n + \Delta m_n, \tag{13}$$

where m_n is the model in the nth iteration and Δm_n is the iteration step:

$$\Delta m_n = -\left(\hat{H}_n + \alpha \hat{I}\right)^{-1}\left[\hat{F}_n^T R + \alpha\left(m_n - m_{\text{apr}}\right)\right]. \tag{14}$$

In the last equation, $\hat{\mathbf{H}}$ is the Hessian matrix given by $\hat{\mathbf{H}} = \hat{\mathbf{F}}^* \hat{\mathbf{F}}$, where $\hat{\mathbf{F}}$ is the Jacobi matrix.

The iteration process is automatically terminated when the normalized misfit reaches the desired value. This is 0.1% for synthetic data. For real data, however, it is set equal to the noise level if it is known. Eq. (5) is used as the forward solution.

The Jacobi matrix is composed of partial derivatives of data with respect to parameters. Thus, the Jacobi matrix is a $N_{\text{d}} \times N_{\text{m}}$ matrix, where N_{d} is the number of data points used and N_{m} is the number of model parameters. Therefore, in our case the Jacobi matrix is a 4×2

matrix, since we have two parameters, depth, d, and conductance, S, and we usually use four data points: $|V(t_1)|$, $|V(t_2)|$, $|V(t_3)|$, $|V(t_4)|$. The Jacobi matrix has the following form:

$$\hat{\mathbf{F}} = \begin{bmatrix} \frac{\partial|V(t_1)|}{\partial d} & \frac{\partial|V(t_1)|}{\partial S} \\ \frac{\partial|V(t_2)|}{\partial d} & \frac{\partial|V(t_2)|}{\partial S} \\ \frac{\partial|V(t_3)|}{\partial d} & \frac{\partial|V(t_3)|}{\partial S} \\ \frac{\partial|V(t_4)|}{\partial d} & \frac{\partial|V(t_4)|}{\partial S} \end{bmatrix}. \quad (15)$$

The elements of the Jacobi matrix are computed analytically, by differentiating Eq. (5) with respect to depth, d, and conductance, S:

$$\frac{\partial|V|}{\partial d} = -\frac{3M\Sigma n}{4\pi S}\frac{1}{(d+\tau)^5}, \quad (16)$$

$$\frac{\partial|V|}{\partial S} = \frac{3M\Sigma n}{4\pi\mu_o S^3}\frac{t}{(d+\tau)^5} - \frac{3M\Sigma n}{16\pi S^2}\frac{1}{(d+\tau)^4}. \quad (17)$$

An important problem is the calculation of the appropriate value of the regularization parameter, α. We have used an adaptive regularization, which is based on the scaling down of the regularization parameter α after several subsequent iterations (Zhdanov, 1993). If the misfit value happens to increase, the value of α is increased and the iteration step is repeated.

To calculate the starting value of α, we compute the "Frobenius norm" of the Hessian matrix, by adding the squares of all the elements of the matrix and taking the square root of the sum. This norm is then scaled down by a factor of 100 to produce the first value of α. This factor is chosen so that the values of the misfit functional and the stabilizing functional are scaled to be of approximately the same order.

Another critical question in the implementation of the regularized S-inversion method is the selection of the starting model. The regularization is very important in the solution of this problem because it makes the inversion result less dependent on the starting model. Without regularization a small change in the starting model can cause divergence of the inversion algorithm. We have used the following approach to selecting the starting model. First, we use the result produced by the differential S-transformation for the first time delay as the starting model for the inversion of the first "data window". After that, while applying a sliding time window to the data, we use as a starting model the result of the inversion for the previous time window location. This is justified by the fact that theoretically the conductance–depth curve should increase monotonically as time passes and the field penetrates to greater depths in the earth. Moreover, we found that this approach decreases the number of iterations needed to minimize the parametric functional.

After we have determined the depth and conductance values of the thin sheet for every time window, we differentiate the conductance curve with respect to depth, as described in Section 2.1, to obtain the conductivity–depth curve.

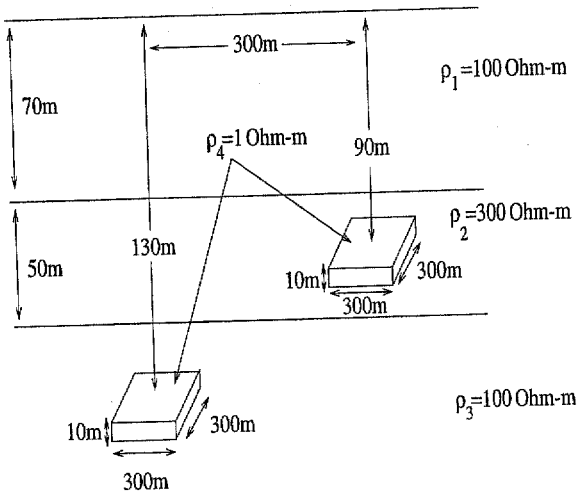

Fig. 3. 3-D model of two conductive bodies in a layered earth.

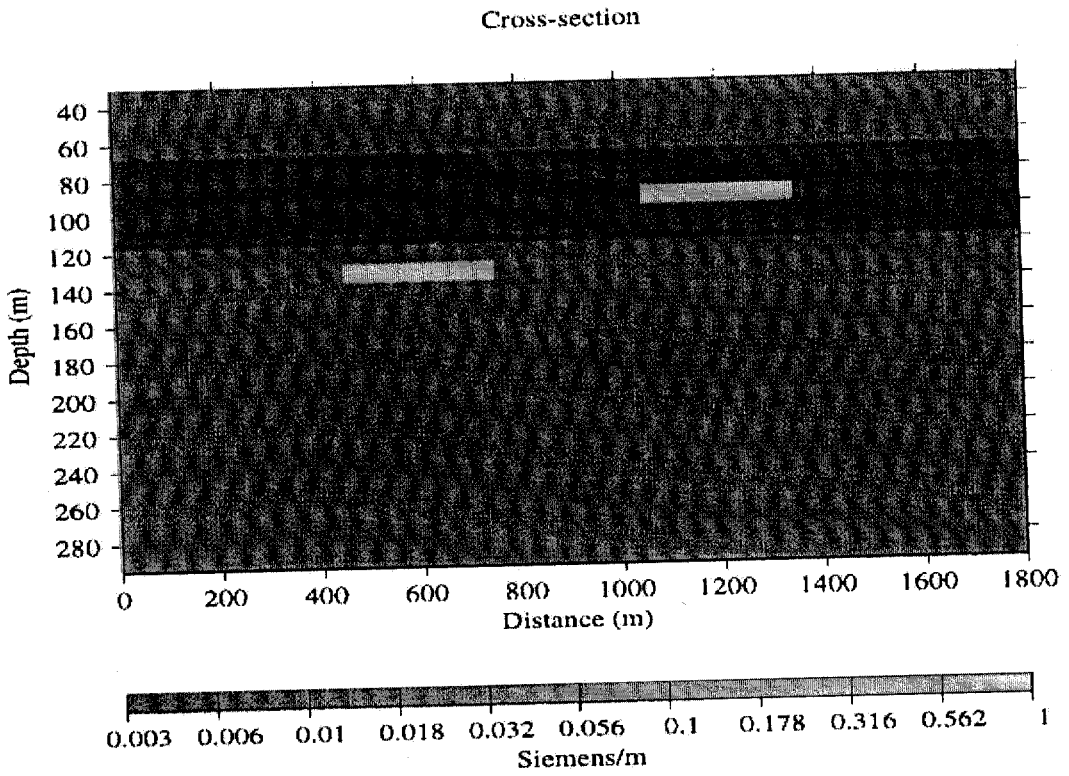

Fig. 4. Cross-section of the model in Fig. 3.

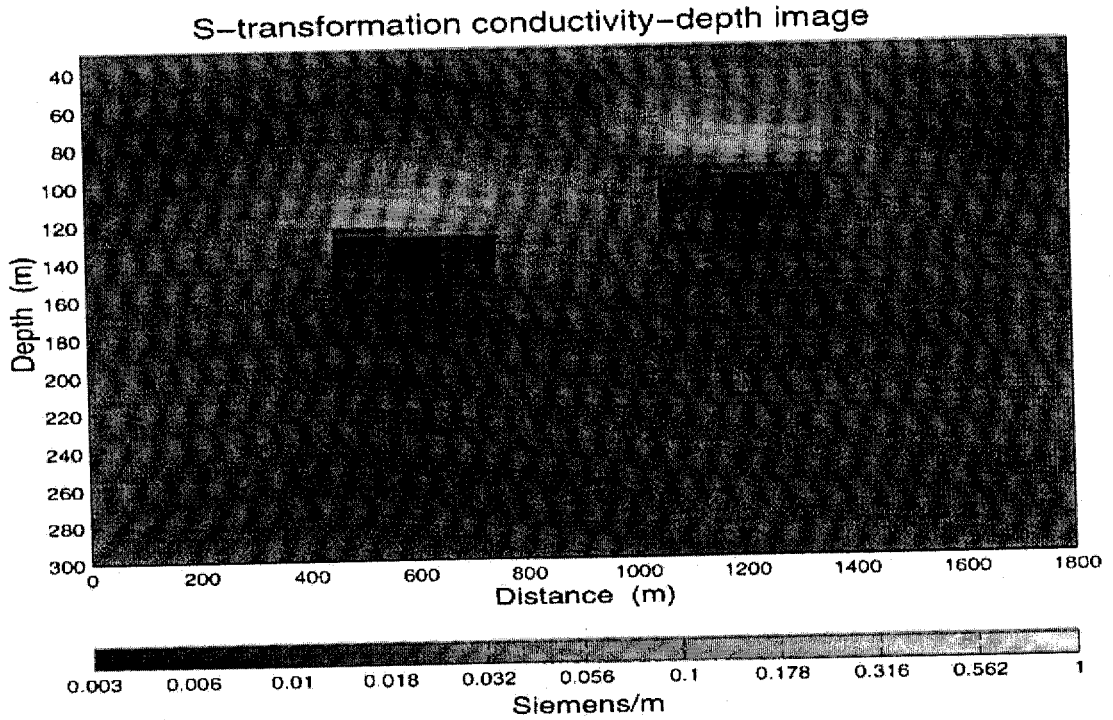

Fig. 5. Conductivity–depth image obtained by differential S-transformation for model in Fig. 3.

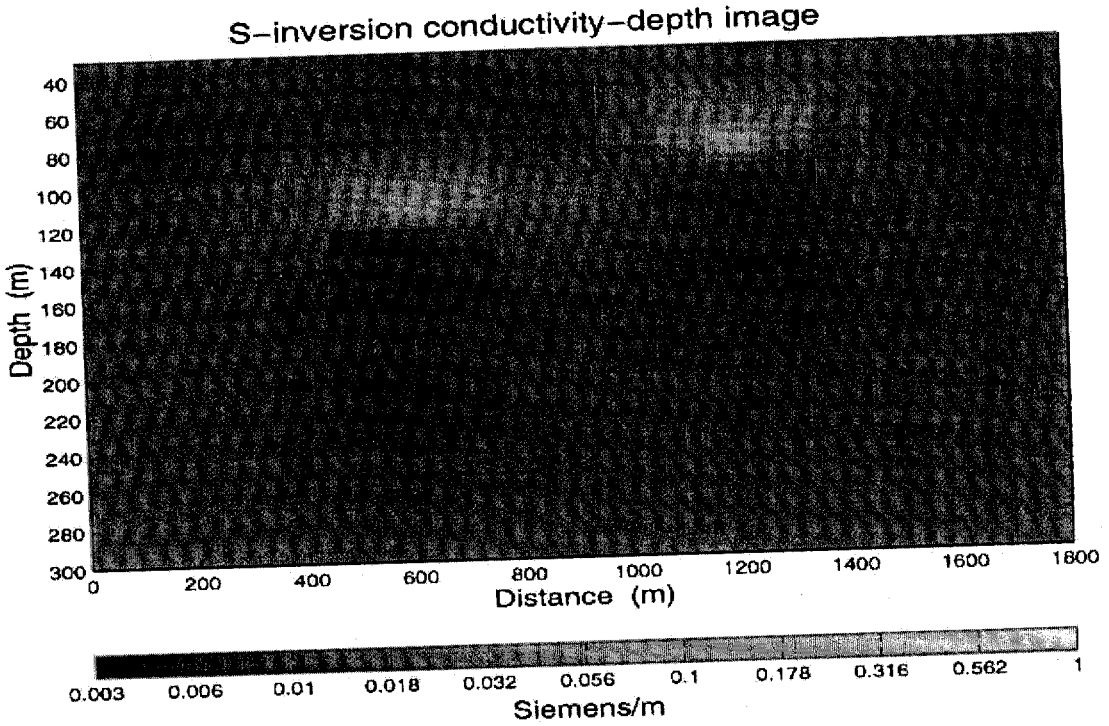

Fig. 6. Conductivity–depth image obtained by regularized S-inversion for model in Fig. 3.

The regularized S-inversion is mathematically rigorous and still very fast, since it uses a simple formula as the forward operator. Moreover, the only differentiation required is that for transforming the conductance–depth profile to the conductivity–depth profile. Note that we apply spatial filtering to make this differentiation stable.

3. Application of S-inversion to 3-D synthetic data interpretation

The set of 3-D models used in this study includes models of local conductive bodies that simulate possible targets for geophysical exploration.

The synthetic TDEM data ($\partial B_z/\partial t$ values) were generated by the 3-D EM forward modeling code SYSEM, developed by Xiong (1992). This code is based on the integral equations method.

The numerical modeling code has been used to simulate a survey in slingram mode with a

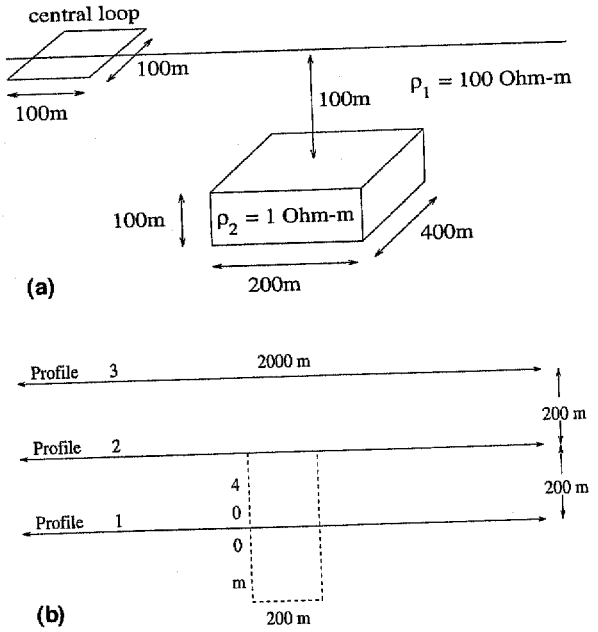

Fig. 7. (a) 3-D model of a thick conductive body in a resistive medium. (b) Plan view of the model in Fig. 7a.

fixed transmitter–receiver separation, where the transmitter and receiver were moving together along the profile and passing above the center of the 3-D structures. It is assumed that the transmitter is excited by a step pulse and the receiver measures the time derivative of the magnetic induction vector.

Fig. 3 shows the first 3-D model used in this study. It consists of two 300 m × 300 m × 10 m bodies with resistivity 1 Ω m embedded in a layered earth. The first body lies at a depth of 90 m and the second at a depth of 130 m from the surface. The distance between them is 300 m. The horizontal layers have thicknesses 70 and 50 m, and resistivities 100 and 300 Ω m, respectively, while the lower half-space has a resistivity of 100 Ω m.

The time interval of observations was between 1 μs and 1 s. Both the transmitter and the receiver were vertical magnetic dipoles simulat-

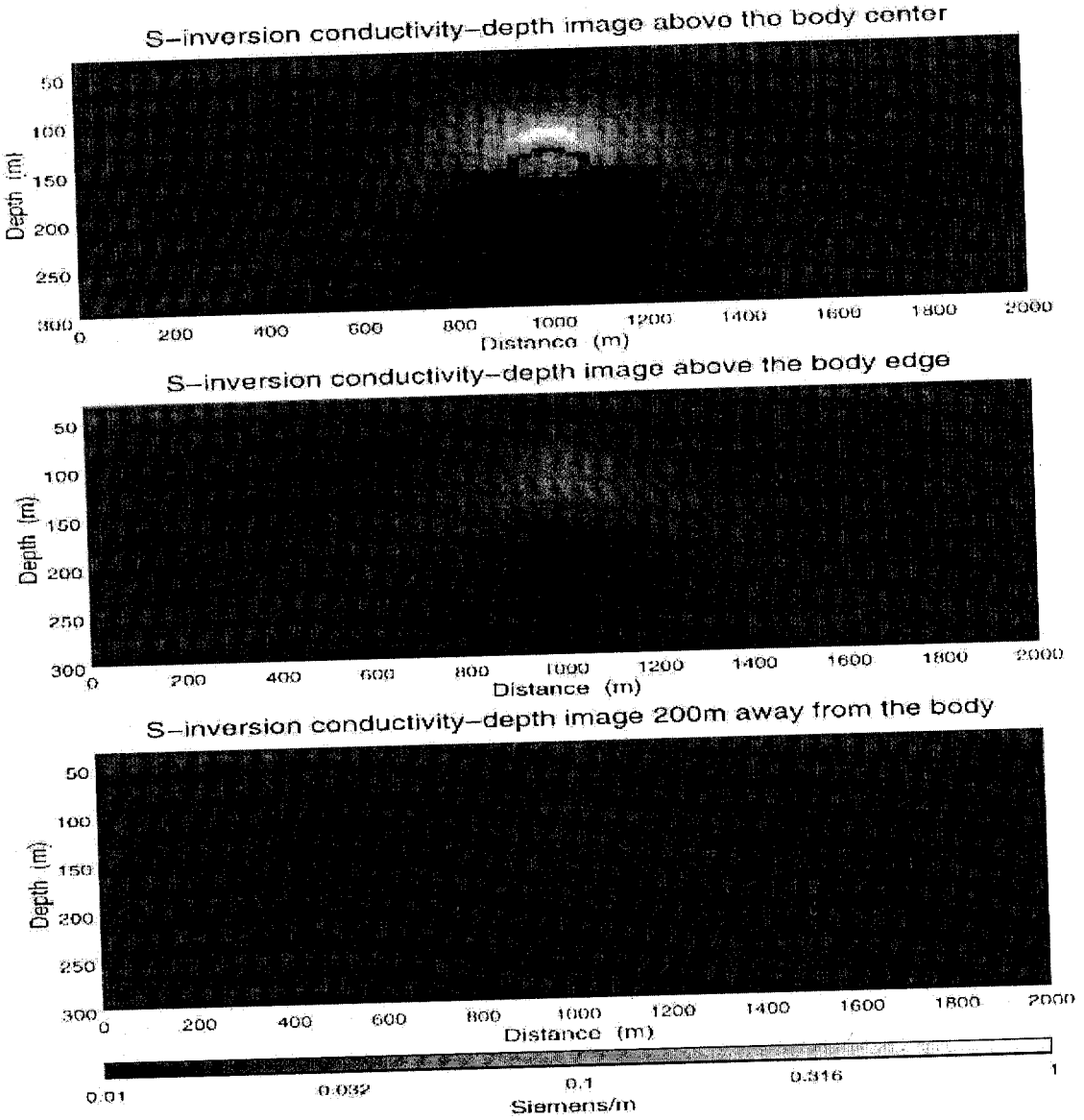

Fig. 8. Conductivity–depth image obtained by the regularized S-inversion for the profile passing above the center of the body in Fig. 7a. (b) Conductivity–depth image obtained by the regularized S-inversion for the profile passing above the edge of the body in Fig. 7a. (c) Conductivity–depth image obtained by the regularized S-inversion for the profile passing 200 m away from the edge of the body in Fig. 7a.

ing horizontal induction loops located at the surface of the earth with 10 m separation. As mentioned, the slingram mode was applied. Fig. 4 shows a cross-section of the model along the profile where measurements were taken every 100 m.

Figs. 5 and 6 represent the conductivity–depth images obtained by the application of the differential S-transformation and the regularized S-inversion at every receiver location. As we can see, the two conductive bodies are satisfactorily imaged, although the retrieved conductivity is lower than the true one. In particular, the differential S-transformation seems to produce conductivity values closer to the true ones, but the regularized S-inversion defines better the lateral extent of the bodies. On the other hand, both techniques resolve correctly the locations of the bodies along the profile, but image the bodies shallower than the true depths. This results from the fact that the overlying layers are not insulating but have a finite resistivity and

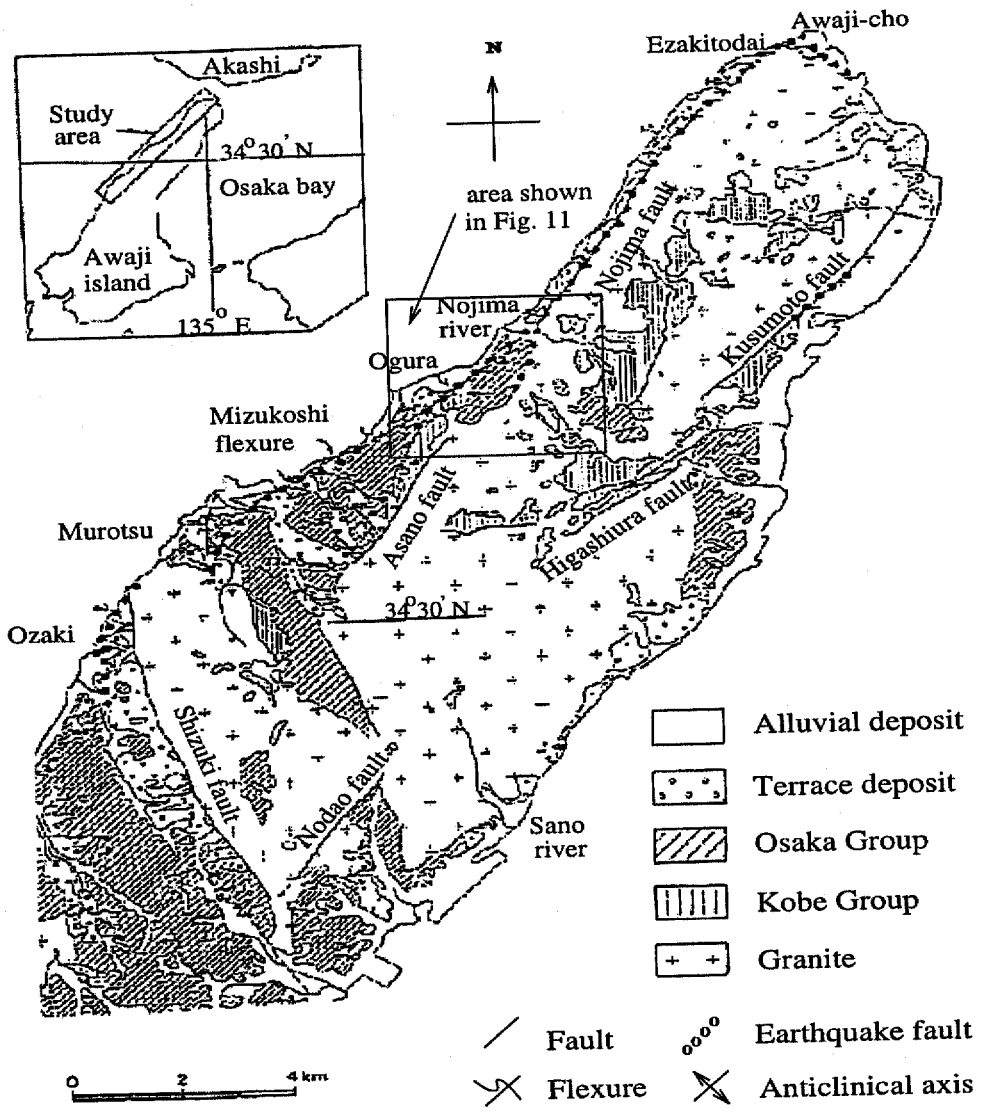

Fig. 9. Geological map of the northern Awaji island after Lin and Uda (1995).

contribute to the total conductance. Note, also, that the resistive layer in the background is not well resolved in this model because S-inversion is based on the thin sheet model which assumes a single conducting thin sheet in an otherwise insulating half-space. Resistive targets such as the second layer in the specific model are difficult to resolve.

The second 3-D model used in this study is shown in Fig. 7a. It consists of a 200 m × 400 m × 100 m body with resistivity 1 Ω m located at a depth of 100 m from the surface in a 100 Ω m resistive host.

The time interval of observations was between 1 μs and 1 s. The central-loop sounding method was simulated. The transmitter was a 100 m × 100 m horizontal rectangular loop and the receiver was a vertical magnetic dipole located at the center of the transmitting loop. Measurements were taken every 25 m along three parallel profiles. The first profile passes above the center of the body, the second above the edge of the body and the third 200 m away from the body (Fig. 7b).

Fig. 8a shows the result of the application of the regularized S-inversion to the measurements taken along the first profile (passing above the body center), Fig. 8b shows the result for the second profile (passing above the edge of the body), and Fig. 8c shows the result for the third profile (passing 200 m away from the body). We can clearly see the presence of the conductive body in the first profile, whereas its effect is significantly diminished in the second profile and has disappeared in the third. The lateral extent of the conductive body is defined quite well as we can see in the first profile, although the 3-D effects are clearly present. The thickness, however, of the body is not completely resolved. Only the upper part of the body is clearly visible. This result is different from the results for the previous 3-D models, where the

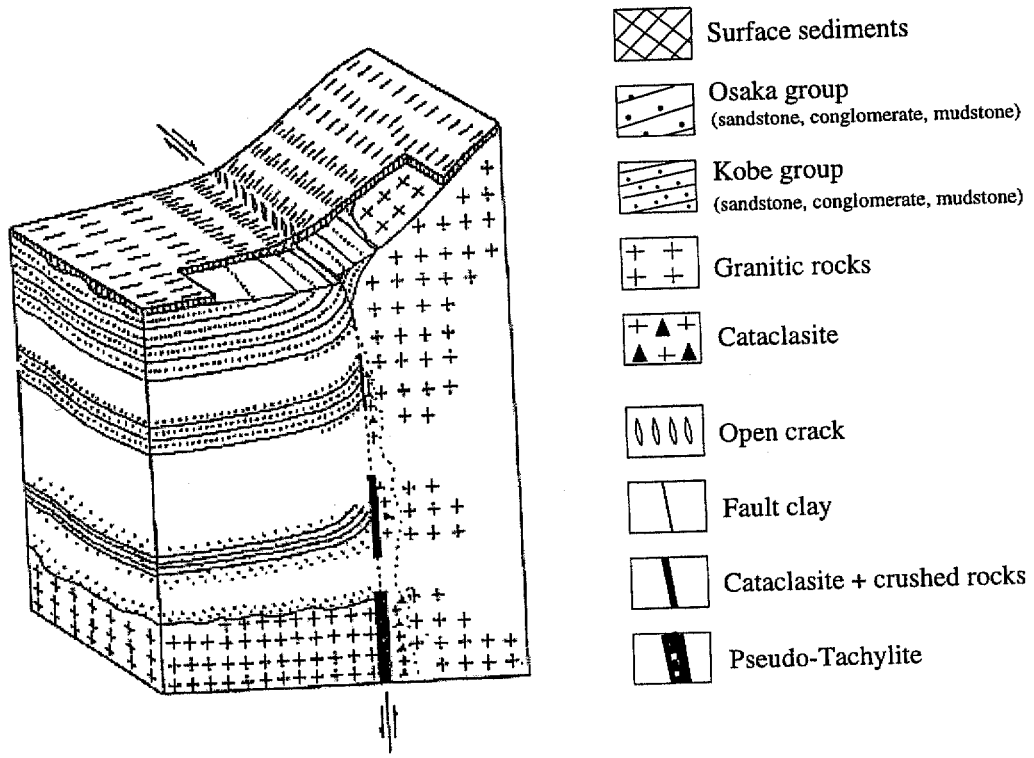

Fig. 10. Schematic view of the geological cross-section of the Nojima fault.

thicknesses of the conductive bodies were resolved quite well. The reason is that in those models the conductive bodies were plate-like thin bodies, which fit better to the thin sheet model. On the other hand, the conductive body of this model is a thick block that has dimensions of the same magnitude and therefore our model departs considerably from the thin sheet model assumption.

In conclusion, based on the results of the above 3-D models, we can say that S-inversion seems to be a reliable and stable method for fast imaging of local conductive targets in a resistive host. However, only the upper part of thick conductors can be successfully resolved. Moreover, the method is not appropriate for locating resistive targets.

4. Case history: interpretation of TDEM data obtained at the Nojima fault zone, Japan

4.1. Geological and seismotectonic data from the survey area

A TDEM survey was conducted by Mindeco's geophysical department across the Nojima active fault zone on Awaji island, Japan. The goal of this survey was to locate the extension of the Nojima fault zone beyond its surface exposure and to estimate the resistivity structure around the active fault.

Awaji island lies off the Kobe bay. Its geology consists of surface sediments, the Osaka group (sandstone, conglomerate, mudstone), the Kobe group (sandstone, conglomerate, mud-

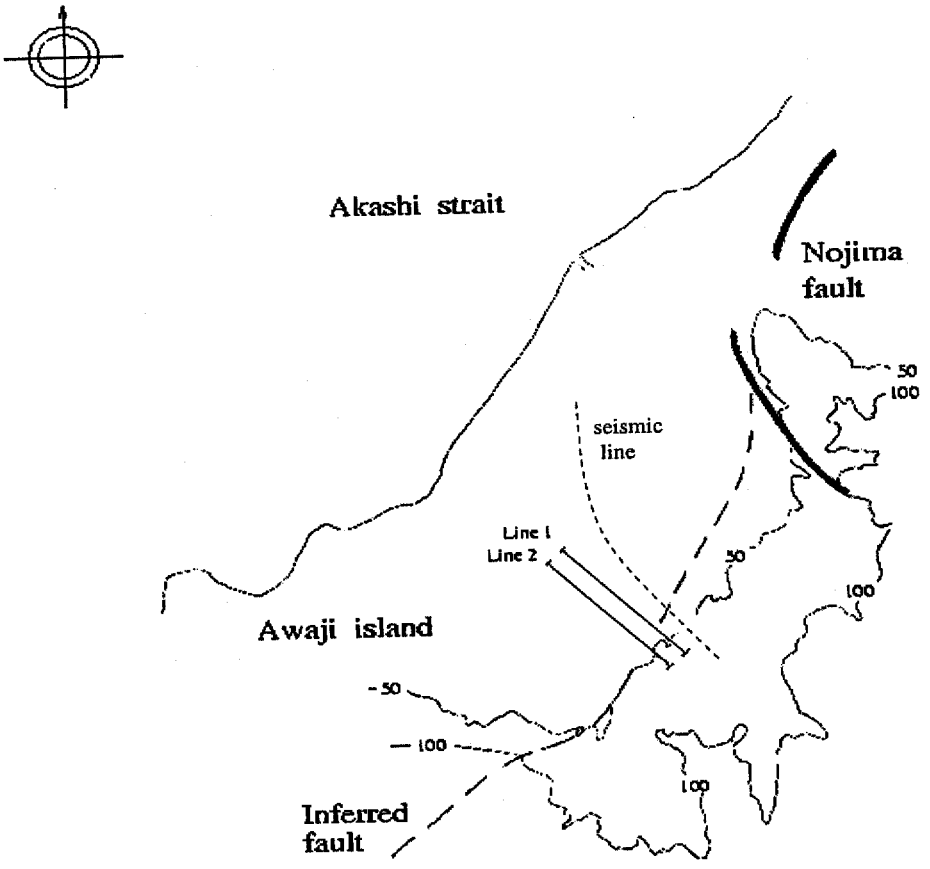

Fig. 11. Location of EM survey lines and seismic line.

stone), and granite (Fig. 9). The Nojima fault is a boundary between Pre-Neogene granitic rocks and the Kobe group and Quaternary deposits, and lies between a basin and a hill. The schematic view of the geological cross-section of the location of the Nojima fault is given in Fig. 10.

The area is seismically very active. Besides the Nojima fault, there are a number of other Quaternary right-lateral faults (Rokko fault zone) running from Awaji island to Kobe with NE–SW strike. The latest big earthquake in the area was the 7.2 earthquake that occurred on January 17, 1995, and is best known as the

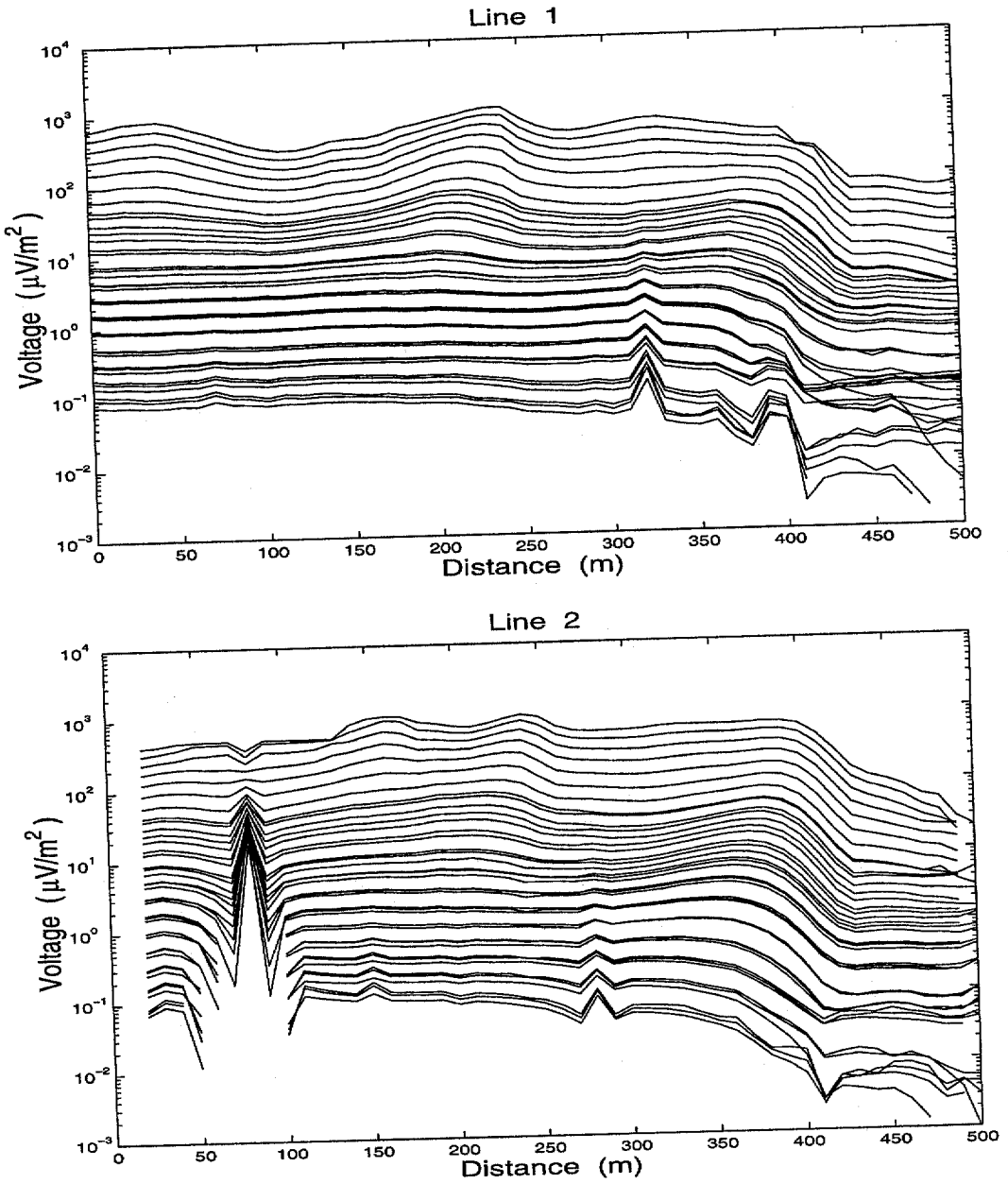

Fig. 12. (a) TDEM data obtained along line 1. Lines correspond to different time delays, ranging from 13 to 545 μs. (b) TDEM data obtained along line 2. Lines correspond to different time delays, ranging from 13 to 545 μs.

"Kobe earthquake". The epicenter was close to the city of Kobe (population about 1.4 million), approximately 200 km away from the Nankai trough (the major plate boundary between the Philippine Sea and the Eurasia plates), and about 40 km from the Median Tectonic Line (Lin and Uda, 1995). In this sense the earthquake was an intraplate earthquake (Kanamori, 1995). The Nojima earthquake fault with a length of 18 km appeared along the northwestern coastal line on

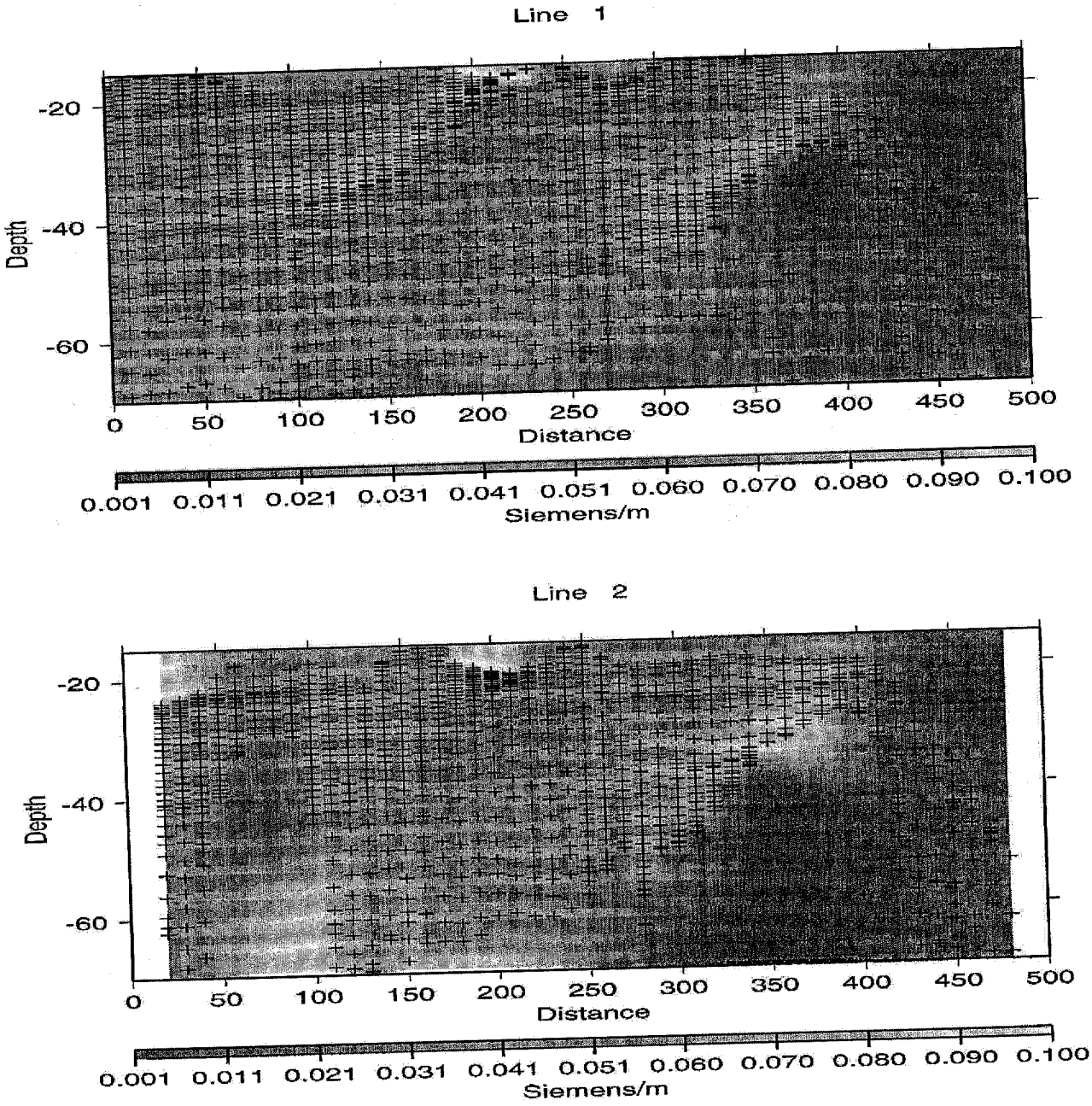

Fig. 13. (a) Conductivity–depth image along line 1 produced using regularized S-inversion. Crosses indicate the actual location of S-inversion results. (b) Conductivity–depth image along line 2 produced using regularized S-inversion. Crosses indicate the actual location of S-inversion results.

the Awaji island in that earthquake. The main fault rupture propagated southwestward from the epicenter along the Nojima fault during the earthquake. This fault is one of the most active in Japan with an average displacement of more than 1 mm/year.

4.2. Survey design and data description

The TDEM survey conducted by Mindeco runs across the inferred Nojima fault zone (Fig. 11). It consisted of two profiles, about 500 m long, set nearly perpendicular to the inferred fault zone, striking WNW–ESE. The separation of the profiles was 60 m. Central-loop soundings were conducted at an interval of 10 m along the profiles. The transmitting loop size was 60 m × 60 m. The receiver was a vertical component sensor coil with 31.4 m^2 effective area, located at the center of the loop. A PROTEM instrument supplied by Geonics was used for the measurements. The transmitter current was 2.5 A with a bipolar rectangular current wave form with a 50% duty cycle. Finally, data were recorded in three overlapping time ranges from approximately 6 μs to 7 ms.

4.3. Application of S-inversion for fast imaging of the TDEM data

Before S-inversion was actually applied to the data set, we discarded all data with signal-to-noise ratio less than 1, keeping data for times less than 500 μs. The data from line 1 and line 2 are shown in Fig. 12a and b, respectively.

We then applied the S-inversion to every receiver location and used a 2-D interpolation to create a conductivity–depth image for every profile. Fig. 13a and b show these images. There is a clear change in the conductivity at the right (SE) end of all lines, which indicates the transition from the conductive sediments (on the left) to the resistive granite (on the right). This transition corresponds to the location of the Nojima fault. The fault, down to the first 70 m of depth where we have S-inversion results, seems to be nonvertical but it is rather dipping NW (to the left in the image). Moreover, there appears to be another interesting feature, a ''weak'' conductive zone in the middle of the profiles. This zone delineates another possible faulting zone in the subsurface that is not visible from the surface morphology.

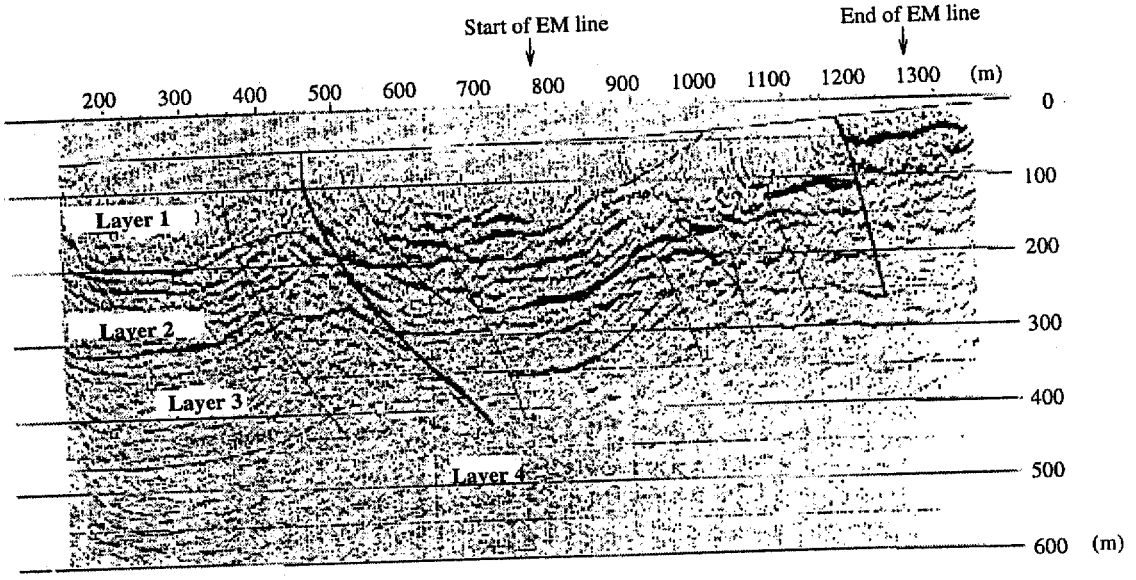

Fig. 14. Seismic cross-section for the survey area.

The conductivity–depth images retrieved by the S-inversion can be compared with a cross-section created for the same area by a seismic geophysical survey, shown in Fig. 14. The seismic line lies a short distance away from the EM lines and for the most part runs parallel to line 1 of the TDEM survey (Fig. 11). It can be seen that the two cross-sections agree quite well down to the depth of about 70 m, where S-inversion results extend. In particular, the conductive zone shown approximately in the middle of the profiles is found exactly at the same point on the seismic cross-section as a possible faulting zone. The Nojima fault zone is shown to be almost vertical on the seismic cross-section. However, we should keep in mind that the S-inversion results extend only down to a depth of about 70 m and do not give us any information about the dip of the fault at greater depths.

The results we have obtained suggest that S-inversion can be useful in delineating faulting zones and imaging changes in the subsurface conductivity distribution around the Nojima fault zone. Furthermore, the reliability of the method was enhanced by the fact that these results agree quite well with those of a seismic survey conducted earlier in the same area.

5. Conclusions

In conclusion, S-inversion is an efficient and stable method for fast imaging of TDEM data that successfully locates anomalous conductive zones in the subsurface. It especially provides good resolution of local conductive objects in resistive environments. Furthermore, it is extremely fast because it does not require repetitive costly forward modeling. It should be noted, however, that S-inversion is an imaging technique, not a full conventional inversion. Therefore, it is an approximate method and its results could be used as initial values for subsequent more rigorous inversion.

The method of course has limitations. It cannot resolve well the resistive targets because the whole technique is based on the thin sheet model assumption. Moreover, the more conductive the host of the conductive target is, the more our results will tend to underestimate the depth of the conductive target. Finally, only the upper part of thick conductors can be successfully resolved.

Application of S-inversion for the fast imaging of 3-D synthetic and real TDEM data shows that the method is stable and reliable even in complicated environments and can provide useful information about the subsurface conductivity distribution.

The Nojima fault zone is clearly shown on the conductivity–depth images obtained by the S-inversion. The fault is located on the right-hand (SE) side of the images and seems to be dipping to the left (NW). It separates the more conductive sediments on the left from the resistive granite on the right. Another conductive zone that could represent a possible faulting zone was located approximately in the middle of the profiles.

Acknowledgements

The authors acknowledge the support of the University of Utah Consortium for Electromagnetic Modeling and Inversion (CEMI), which includes Advanced Power Technologies, Baker Atlas Logging Services, BHP Minerals, EXXON Production Research, INCO Exploration, Japan National Oil Corporation, MINDECO, MOBIL Exploration and Production Technical Center, Naval Research Laboratory, Newmont Gold, Rio Tinto, Shell International Exploration and Production, Schlumberger-Doll Research, Unocal Geothermal, and Zonge Engineering. We especially want to thank Mindeco, Japan, for providing us with the TDEM field data. Finally, the first author wishes to thank the State Scholarships Foundation of Greece for providing partial financial support for this work.

References

Asten, M.W., 1998. On the use of conductance and differential conductivity in TEM parasections (CDI). 68th Ann. Int. Mtg., Soc. Expl. Geophys., Expanded Abstracts, pp. 421–424.

Barnett, C.T., 1984. Simple inversion of time-domain electromagnetic data. Geophysics 49, 925–933.

Berdichevsky, M.N., Zhdanov, M.S., 1984. Advanced Theory of Deep Geomagnetic Sounding. Elsevier, Amsterdam.

Eaton, P.A., Hohmann, G.W., 1989. A rapid inversion technique for transient electromagnetic soundings. Physics of the Earth and Planetary Interiors 53, 384–404.

Fullagar, P.K., 1989. Generation of conductivity–depth parasections from coincident loop and in-loop TEM data. Exploration Geophysics 20, 43–45.

Kanamori, H., 1995. The Kobe (Hyogo-ken Nanbu), Japan, earthquake of January 16, 1995. Seismological Research Letters 66, 6–10.

Lee, T., 1977. Estimation of depth to conductors by the use of electromagnetic transients. Geophysical Prospecting 25, 61–75.

Lin, A., Uda, S., 1995. Segmentation and rupture propagation of the Nojima earthquake fault. Zisin 2 (48), 375–386, in Japanese, with English Abstr.

Liu, G., Asten, M., 1993. Conductance–depth imaging of airborne TEM data. Exploration Geophysics 24, 655–662.

Macnae, J., Lamontagne, Y., 1987. Imaging quasi-layered conductive structures by simple processing of transient electromagnetic data. Geophysics 52, 545–554.

Nabighian, M.N., 1979. Quasi-static transient response of a conducting half-space — an approximate representation. Geophysics 44, 1700–1705.

Nekut, A.G., 1987. Direct inversion of time-domain electromagnetic data. Geophysics 52, 1431–1435.

Price, A.T., 1949. The induction of electric currents in non-uniform thin sheets and shells. Quarterly Journal of Mechanics and Applied Mathematics 2, 283–310.

Raiche, A.P., Gallagher, R.G., 1985. Apparent resistivity and diffusion velocity. Geophysics 50, 1628–1633.

Sheinmann, S.M., 1947. On specification of electromagnetic fields in the Earth. Prikladnaya Geofizika 3, 3–57, in Russian.

Sidorov, V.A., Tikshaev, V.V., 1969. Electrical Prospecting with Transient Field in Near Zone, Saratov University, USSR.

Singer, B.S., Green, A., 1998. Generalisation of the transient field solution for a thin layer of finite thickness. Exploration Geophysics 29, 195–198.

Smith, R.S., Edwards, R.N., Buselli, G., 1994. An automatic technique for presentation of coincident-loop, impulse-response, transient, electromagnetic data. Geophysics 59, 1542–1550.

Tartaras, E., Zhdanov, M.S., 1996. Fast S-inversion in the time domain: method of interpretation using the thin sheet approach. 66th Ann. Int. Mtg., Soc. Expl. Geophys., Expanded Abstracts, pp. 1306–1309.

Wolfgram, P., Karlik, G., 1995. Conductivity–depth transform of GEOTEM data. Exploration Geophysics 26, 179–185.

Xiong, Z., 1992. Electromagnetic modelling of three-dimensional structures by the method of system iterations using integral equations. Geophysics 57, 1556–1561.

Zhdanov, M.S., 1993. Regularization in Inversion Theory, Tutorial, Colorado School of Mines.

Zhdanov, M.S., Keller, G.V., 1994. The Geoelectrical Methods in Geophysical Exploration. Elsevier, Amsterdam.